AFRL-ML-WP-TR-2004-4008

PROCESSING, MICROSTRUCTURES, AND PROPERTIES OF Nb-BASED METAL/SILICIDE ALLOYS

Madan G. Mendiratta

UES, Inc.
4401 Dayton-Xenia Road
Dayton, OH 45432-1894

JULY 2003

Interim Report for 01 June 2001 – 01 June 2003

Approved for public release; distribution is unlimited.

STINFO INTERIM REPORT

MATERIALS AND MANUFACTURING DIRECTORATE
AIR FORCE RESEARCH LABORATORY
AIR FORCE MATERIEL COMMAND
WRIGHT-PATTERSON AIR FORCE BASE, OH 45433-7750

NOTICE

USING GOVERNMENT DRAWINGS, SPECIFICATIONS, OR OTHER DATA INCLUDED IN THIS DOCUMENT FOR ANY PURPOSE OTHER THAN GOVERNMENT PROCUREMENT DOES NOT IN ANY WAY OBLIGATE THE U.S. GOVERNMENT. THE FACT THAT THE GOVERNMENT FORMULATED OR SUPPLIED THE DRAWINGS, SPECIFICATIONS, OR OTHER DATA DOES NOT LICENSE THE HOLDER OR ANY OTHER PERSON OR CORPORATION; OR CONVEY ANY RIGHTS OR PERMISSION TO MANUFACTURE, USE, OR SELL ANY PATENTED INVENTION THAT MAY RELATE TO THEM.

THIS REPORT HAS BEEN REVIEWED BY THE OFFICE OF PUBLIC AFFAIRS (ASC/PA) AND IS RELEASABLE TO THE NATIONAL TECHNICAL INFORMATION SERVICE (NTIS). AT NTIS, IT WILL BE AVAILABLE TO THE GENERAL PUBLIC, INCLUDING FOREIGN NATIONS.

THIS TECHNICAL REPORT HAS BEEN REVIEWED AND IS APPROVED FOR PUBLICATION.

/s/

WYNN SANDERS, Capt, USAF Project Engineer
Metals Branch
Metals, Ceramics & NDE Division

/s/

ROLAND DUTTON, Chief
Metals Branch
Metals, Ceramics & NDE Division

/s/

GERALD J. PETRAK, Asst Chief
Metals, Ceramics & NDE Division
Materials & Manufacturing Directorate

IF YOUR ADDRESS HAS CHANGED, IF YOU WISH TO BE REMOVED FROM OUR MAILING LIST, OR IF THE ADDRESSEE IS NO LONGER EMPLOYED BY YOUR ORGANIZATION, PLEASE NOTIFY, AFRL/MLLM, WRIGHT-PATTERSON AFB, OH 45433-7817 TO HELP US MAINTAIN A CURRENT MAILING LIST.

COPIES OF THIS REPORT SHOULD NOT BE RETURNED UNLESS RETURN IS REQUIRED BY SECURITY CONSIDERATION, CONTRACTUAL OBLIGATIONS, OR NOTICE ON A SPECIFIC DOCUMENT.

REPORT DOCUMENTATION PAGE

Form Approved
OMB No. 0704-0188

1. REPORT DATE *(DD-MM-YY)*	2. REPORT TYPE	3. DATES COVERED *(From - To)*
July 2003	Interim	06/01/2001 – 06/01/2003

4. TITLE AND SUBTITLE
PROCESSING, MICROSTRUCTURES, AND PROPERTIES OF Nb-BASED METAL/SILICIDE ALLOYS

5a. CONTRACT NUMBER
F33615-01-C-5214

5b. GRANT NUMBER

5c. PROGRAM ELEMENT NUMBER
61102F

6. AUTHOR(S)
Madan G. Mendiratta

5d. PROJECT NUMBER
2306

5e. TASK NUMBER
A3

5f. WORK UNIT NUMBER
02

7. PERFORMING ORGANIZATION NAME(S) AND ADDRESS(ES)

UES, Inc.
4401 Dayton-Xenia Road
Dayton, OH 45432-1894

8. PERFORMING ORGANIZATION REPORT NUMBER

9. SPONSORING/MONITORING AGENCY NAME(S) AND ADDRESS(ES)
Materials and Manufacturing Directorate
Air Force Research Laboratory
Air Force Materiel Command
Wright-Patterson AFB, OH 45433-7750

10. SPONSORING/MONITORING AGENCY ACRONYM(S)
AFRL/MLLM

11. SPONSORING/MONITORING AGENCY REPORT NUMBER(S)
AFRL-ML-WP-TR-2004-4008

12. DISTRIBUTION/AVAILABILITY STATEMENT
Approved for public release, distribution is unlimited.

13. SUPPLEMENTARY NOTES

14. ABSTRACT

The Nb-Ti-Cr-Si-X alloys (X=Hf, Al, Sn, Fe, Ge) consisting of the solid solution Nb phase (Nb_{ss}) in equilibrium with intermetallic phases ($(NbTi)_5Si_3$ and Cr_2Nb) are potential candidates as hot-section materials for jet engines. The processing–microstructure–mechanical property relationship and damage/fracture mechanisms of these alloys have been investigated. Processing methods have included induction skull melting, rapidly solidified powder production by rotating electrode and gas-atomization processes, and thermomechanical processing involving hipping and hot-extrusions. Tensile, compressive, and toughness properties have been determined from room temperature to 1100 °C in laboratory air atmosphere. The alloys exhibited a brittle-to-ductile transition at temperatures above 800 °C. Below this temperature, premature brittle tensile failure was caused by large silicide agglomerates at fracture stress values <390 MPa. At 1000 °C, the yield strengths, depending upon composition, ranged from 185 to 372 MPa, while at 1100 °C, they ranged from 138 to 219 MPa. The toughness values ranged from ~10 – 17 MPavm from room temperature to 1100 °C.

15. SUBJECT TERMS
Nb/Nb Silicide Alloys, Induction Skull Melting, Gas-atomization and Plasma Rotating Electrode Powder Processing, Processing-microstructure-property Relations, Fracture Strength and Toughness

16. SECURITY CLASSIFICATION OF:			17. LIMITATION OF ABSTRACT:	18. NUMBER OF PAGES	19a. NAME OF RESPONSIBLE PERSON (Monitor)
a. REPORT	b. ABSTRACT	c. THIS PAGE			CAPT Wynn Sanders
Unclassified	Unclassified	Unclassified	SAR	46	19b. TELEPHONE NUMBER *(Include Area Code)* (937) 255-1351

TABLE OF CONTENTS

LIST OF FIGURES

LIST OF FIGURES (CONT.)

LIST OF FIGURES (CONC.)

LIST OF TABLES

FOREWORD

The work presented in this report was supported by Air Force Contract F33615-01-C-5214, and Captain Wynn Sanders of the Materials Development Branch, AFRL/MLL, was the Government Project Engineer. The research reported herein covered the period 1 June 2001 to 1 June 2003.

1. Introduction

Under the Integrated High Performance Turbine Engine Technology (IHPTET) Program, alloys within the Nb-Ti-Cr-Si-Hf-X system are being developed for advanced aircraft engine hot-section components. The alloys in this system are refractory metal-toughened, intermetallic-strengthened, multi-phase materials; they consist of a b.c.c. solid-solution metallic β phase in equilibrium with Nb- and Ti-silicides and a small volume fraction of Laves Cr_2Nb phase. For the past several years UES, in parallel with the external GE CRD programs, has been conducting research on phase-relations, oxidation mechanisms and properties on these material systems [1,2,3]. More recently the focus of UES effort has been the processing of these materials in sufficient quantities to enable further evaluation of engineering properties and to perform mechanistic research on mechanical behavior. The processing methods have included induction skull melting (ISM), production of rapidly solidified prealloyed powders using rotating electrode (PREP) and gas-atomization processes and thermomechanical processing involving hipping and hot-extrusions. Important aspects of this investigation are: i) characterization of microstructural evolution as a result of different processing and heat treatments and ii) the relationship of composition-processing-microstructure-mechanical property relations. Mechanical properties have included tensile, compressive and toughness properties from room temperature to 1100°C. Extensive fractographic analysis has been carried out to understand the damage and fracture mechanisms.

2. Composition Selection:

Over the past several years the alloying efforts in the Nb-based alloys, both at UES and GE CRD, have been mainly focussed on phase relations, microstructural evolution and improving the oxidation resistance. Only limited work has been done to investigate the effect of

composition and microstructure on mechanical properties such as strength, ductility, fracture toughness and creep resistance. A single composition has not been discovered which provides an optimal combination of properties for a specific hot-section component e.g., turbine blade. However, the alloying efforts to date exhibit certain compositional trends, which might provide a reasonable combination of properties. Therefore, in consultation with GE CRD, and based upon these compositional trends, a number of alloys were selected to learn how to process these materials. The selected aim compositions, in atomic %, are given in Table I.

Table I
Selected Alloy Compositions (At%)

	Nb	Ti	Cr	Fe	Hf	Si	Ge	Al	Sn
# 1	46.8	21.5	6	3	2	12.5	5	2	1.2
# 2	44.8	19.5	13	-	2	17.5	-	2	1.2
# 3	46.8	21.5	9	-	2	17.5	-	2	1.2

It can be seen from Table I, that the ratio of Nb/Ti is slightly greater than 2; earlier work at GE CRD has shown that a ratio of ≥2 with all other elements having similar levels, provides the lowest minimum creep rates. Additions of Cr + Fe or Cr produces Laves Cr_2Nb phase which is shown to be beneficial for oxidation resistance. The Si and Si + Ge contents around 17% provide good creep and oxidation resistance.

3. Cast Ingot Processing:

The selected alloys were made into cast ingots (6.35 cm diam. x 35.6 cm long) by an induction skull melting (ISM) process by Flowserve, Dayton Ohio. A new crucible and induction coil were designed to allow melting of high-melting temperature elements comprising of these alloys. Appropriate mixtures of master alloys were used; the crucible has capacity to hold a total charge of ~ 25 lb. After melting, the molten mass was cast into insulated graphite

molds. The cast ingots were x-ray radiographed by Flowserve to examine presence of gross porosity; in all ingots a center-line region (~ 1 cm diam) was found to exhibit shrinkage porosity.

For each ingot, chemical analyses were carried out on specimens machined from top, middle and bottom of the ingots. At each location, the samples were from a site, which was roughly half way from the center and surface of an ingot. The target and analysed chemistries of the major elements, the range of analyzed interstitial impurities (O, N, C) and trace impurities are given in Table II.

Table II
Aim vs. Analysed Chemistries of Selected Alloys (At%)

# 1	Nb	Ti	Cr	Fe	Hf	Si	Ge	Al	Sn
AIM	46.8	22.5	6	3	2	12.5	5	2	1.2
ANALYSED	45	22.9	7.3	3.7	2.1	12.8	1.06	2.63	1.38

# 2	Nb	Ti	Cr	Hf	Si	Al	Sn
AIM	44.8	19.5	13	2	17.5	2	1.2
ANALYSED	43.2	21.4	14.3	2.1	14.4	2.4	1.25

# 3	Nb	Ti	Cr	Hf	Si	Al	Sn
AIM	46.8	21.5	9	2	17.5	2	1.2
ANALYSED	47.7	22	7.3	1.8	16.8	1.37	1.2

0xygen: - 700 - 900 ppm by weight
Nitrogen: - 150 - 200 ppm by weight
Carbon: - 120 - 120 ppm by weight

Small Metallic Impurities: Zr, Cu, W

In alloy # 1, the analyzed Ge content is much smaller than the aim. In alloy # 2, analysed Si content is smaller while in alloy # 3, the Cr content is smaller than the aim compositions. The information on these major differences in analysed and target compositions was conveyed to Flowserve to device procedures (i.e., different composition of master alloys, compensation for elemental losses) to meet the target compositions in the future melt. In fact based upon this interaction with Flowserve, one more ingot with the same target chemistry as # 1 alloy was cast;

Table III includes the aim and analyzed chemistry of the new ingot. It can be seen the analyzed and the aim chemistries are reasonable close to each other.

4. Powder Processing:

In addition to making cast ingots, powder metallugy route was also explored in processing the Nb-based material. The thinking was that the powder processing might result in a fine and homogeneous microstructure, thereby providing flexibility in the range of compositions with higher volume fractions of intermetallic phases supposedly good for creep and oxidation resistance. If upon consolidation/heat treatments these phases do not coarsen significantly, then it is possible that a debit in fracture-critical properties associated with these phases may not be significant. For the powders, the composition chosen was same as that for alloy #1. Six electrodes (5 cm diam. x 20 cm long) were cast using ISM process and -35 mesh powders were made by Starmet using plasma rotating electrode process (PREP). The powders were packed in a plastic container in a glove-box with argon partial pressure. The aim chemistry and the analysed chemistry of the as-received powder is given in Table III and it can be seen that these chemistries very close. Although not shown in this table, the interstitial impurity levels (i.e., O, N) in the powder were similar to those in the ingots.

Small quantities of gas-atomized powder were also made by Crucible on alloy chemistry #4. This was done to compare the microstructures in the powders made by PREP and gas-atomization processes. A charge of chunks of unused PREP electrodes (~450 gm) was skull melted in a small crucible and then the melt was gas atomized. A yield of ~ 300 gm of –35 mesh powder was obtained. This was a batch process with weight limitation of the powder yield imposed by the small size of the crucible and formation of alloy skull in the crucible.

Table III
Aim and Analysed Composition of an Additional Ingot and PREP Powder (At%)

# 4	Nb	Ti	Cr	Fe	Hf	Si	Ge	Al	Sn
AIM *	**46.8**	**22.5**	**6**	**3**	**2**	**12.5**	**5**	**2**	**1.2**
ANALYSED	**-**	**20.4**	**6.2**	**2.8**	**2**	**11**	**4.6**	**2.5**	**1.3**

PREP Powders

# 4	**Nb**	**Ti**	**Cr**	**Fe**	**Hf**	**Si**	**Ge**	**Al**	**Sn**
AIM *	**46.8**	**22.5**	**6**	**3**	**2**	**12.5**	**5**	**2**	**1.2**
ANALYSED	**46**	**21.5**	**6.7**	**3.5**	**2**	**11.2**	**4.7**	**2.6**	**1.3**

*Same as #1

5. Hipping, Heat Treatments and Hot-extrusions:

To investigate whether any casting porosity (excluding gross shrinkage porosity in the center of ISM ingots) can be removed, a sample from ingot #2 was hipped at 1400°C/96h/210MPa argon pressure. Back-scattered electron (BSE) SEM micrographs of Fig. 1 show the results of hipping. Fig. 1(a) shows presence of isolated large pores (~25 μm). But, in the main small pores or crack-like features were seen in the intermetallic phases Fig. 1(b) and (c). Thus, even after this reasonably aggressive hipping cycle, defects remained in the sample. It is possible that a higher temperature/higher pressure hipping may remove these defects, however, this has not been tried.

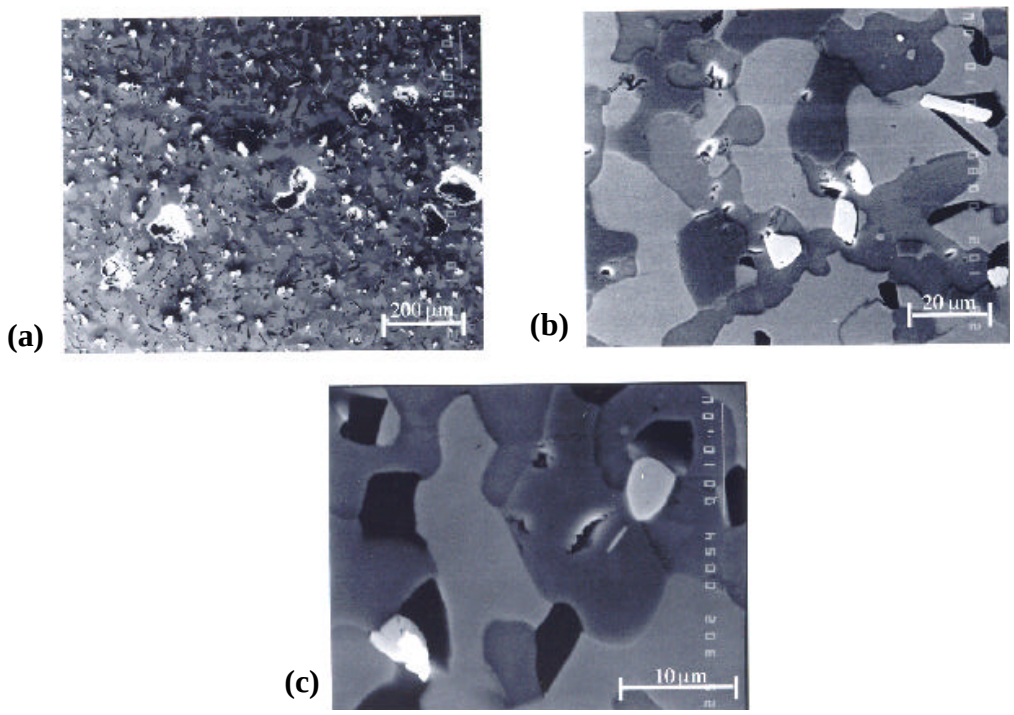

Figure 1. Effect of hipping (1400°C/96h/210MPa Argon Pressure) on porosity in alloy #2 (Table II). Large pores are seen in (a), and intermetallic phases contain crack like defects and small pores, (b) and (c).

The as-cast ingots were subjected homogenization heat treatments (HT). Initially, alloy # 1 was HTed at 1400°C/100h under a partial argon pressure; this resulted in melting of a small portion of surface of the ingot. This may presumably be due to presence of some non-equilibrium phases. Subsequent Ht's involved first a lower temperature step, i.e., 1300°C/24 h followed by an additional HT step of 1400°C/76h. No melting was observed on the samples as a result of these two-step heat treatments. After the HTs, hot-extrusions were carried out either at 1350°C/6:1 ratio or at 1400°C/6:1 ratio. The ingots were canned in 0.635 cm thick Mo cans for the hot-extrusions.

6. Microstructures:

Fig. 2(a-c) shows the BSE SEM micrographs of the as-cast, HTed and extruded (1350°C/6:1 ratio) alloy #1. The as-cast microstructure consists of a fine and uniform mixture of well-dispersed phases. Electron probe microanlysis (EPMA) indicated presence of phase-chemistries corresponding to the solid solution metallic β phase (bright), $(NbTi)_5Si_3$ (gray) phase and the Cr_2Nb (dark) phase. Considerable coarsening occurred as a result of 1400°C/100 h heat treatment (Fig. 2b); EPMA analysis exhibited presence of 4 phases, Table IV.

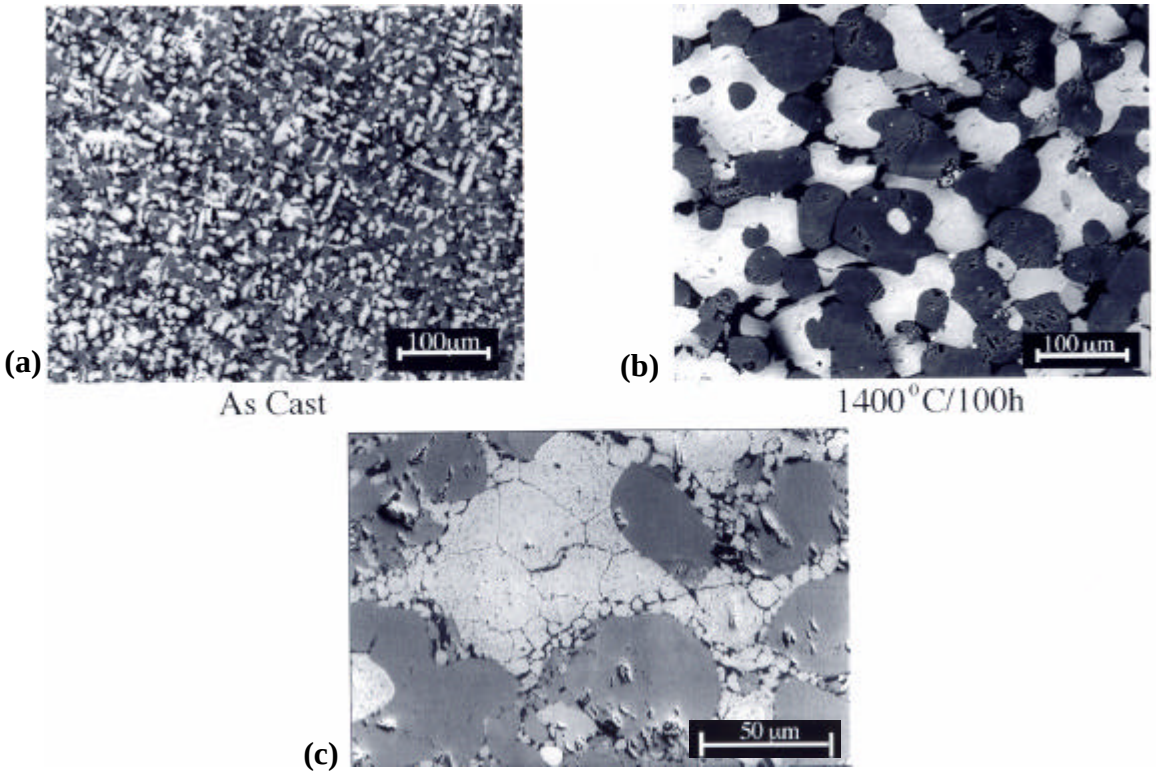

Figure 2. Back-scattered SEM Micrographs exhibiting microstructural development in alloy #1 (Table II) in the (a) as cast, (b) homogenized, and (c) as extruded conditions (1350°C/6:1 Ratio).

Table IV
Phase Chemistry as Revealed by EPMA for Alloy #1 (At%)
7.3Cr - 3.7Fe - 12.8Si -1.06Ge(1400°C/100h)

Element	b Phase	$(NbTi)_5Si_3$	Cr_2Nb	$(TiNb)_5Si_3$
Nb	54.8	38.1	21.28	28.98
Ti	25.1	21.67	17.06	25.55
Cr	9.33	1.94	31.27	1.09
Fe	3.05	2.32	16.71	0.80
Al	3.31	1.92	2.11	1.99
Sn	1.87	0.82	0.01	0.l9
Hf	1.23	2.28	3.23	6.38
Si	1.25	24.8	7.85	28.06
Ge	0.09	6.22	0.48	6.96

A small volume fraction of an additional Ti-rich 5:3 silicide phase (light gray) was also detected. Since there is a significant coarsening as a result of the heat treatment, the 100 h exposure at 1400°C maybe excessive in terms of achieving chemical homogenization. A heat treatment of shorter duration and/or lower temperature may be sufficient to produce homogenization. However, a minimum in heat treatment temperature/time combination to achieve homogenization was not determined.

Fig. 2(c) shows the microstructure corresponding to longitudinal section of the extrusion. The extrusion direction is horizontal in the figure. The β Nb phase appears to have been recrystallized with an intermetallic phase decorating the grain boundaries. The gray silicide phase is not elongated in the extrusion direction and it also did not break up during extrusion. It appears that the silicide phase did not experience significant plastic deformation during hot extrusion.

Fig. 3 (a-d) are the BS SEM micrographs for alloys #2 in as cast, homogenized and hot-extruded conditions, respectively. Because of higher Si content as compared to that in alloy #1, the cast microstructure contains a high volume fraction of the (primary) silicide phase (gray): it is thought, therefore, that this composition is hyper-eutectic with respect to the silicide phase i.e., the primary silicide phase first solidifies in a eutectic mixture. After H.T., 5 phases as revealed

by EPMA were present: β metal solid-solution (light), Nb-rich 5:3 silicide (gray), Ti-rich 5:3 silicide (light gray mostly at the edges of the gray constituent), Cr_2Nb (dark), and $Hf0_2$ (small bright particles).

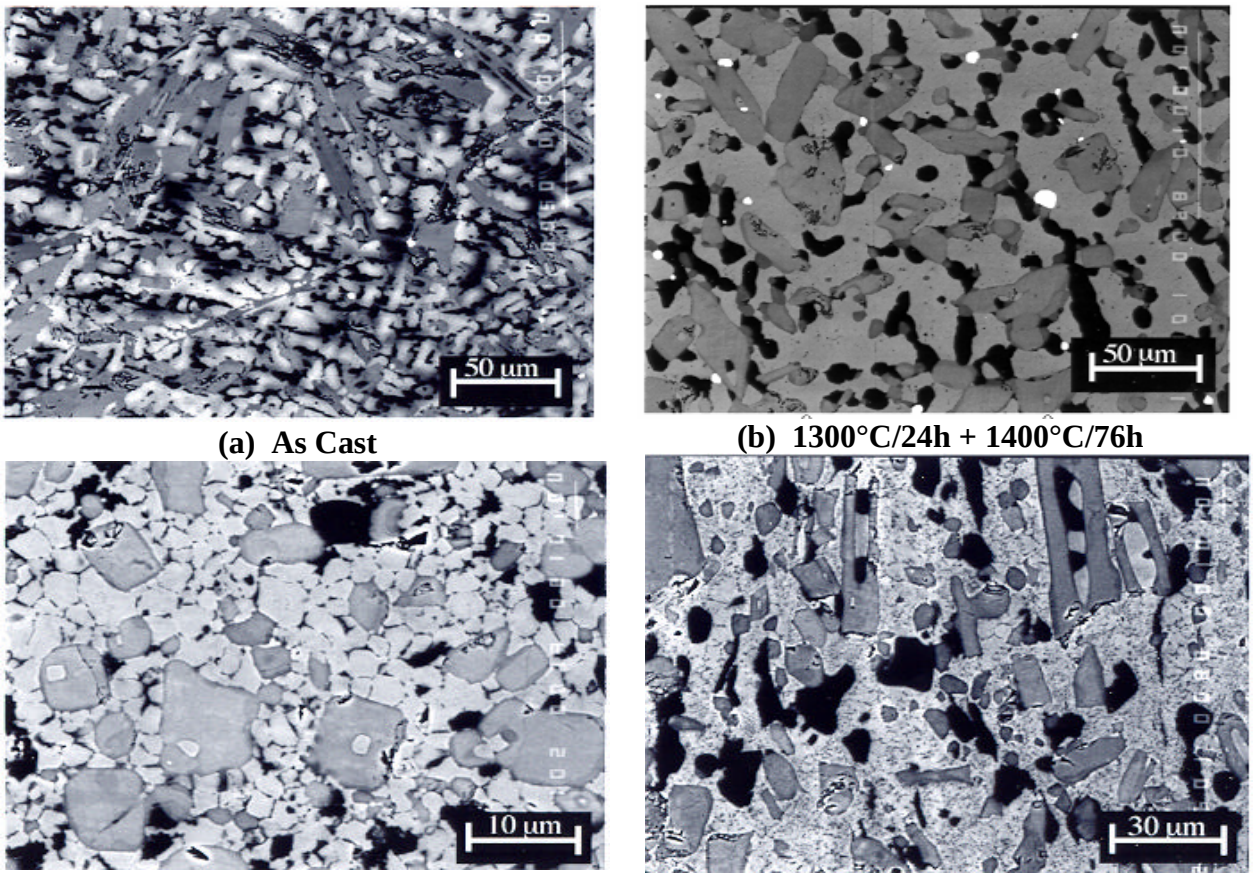

(a) As Cast **(b) 1300°C/24h + 1400°C/76h**

(c) Tran. **(d) Long.**

Homo. + Extruded (1350°C/6:1 R)

Figure 3. Microstructural evolution in alloy # 2 (Table II) in the (a) as cast, (b) homogenized, and (c) and (d) hot-extruded conditions (1350°C/6:1 ratio).

The EPMA data for the phase chemistries are given in Table V.

Table V
Phase Chemistry as Revealed by EPMA for Alloy #2 (At%)

14.3Cr – 14.4 Si (1400°C/100h)

Element	bPhase	$(NbTi)_5Si_3$	Cr_2Nb	$(TiNb)_5Si_3$
Nb	48.86	45.11	23.48	40.55
Ti	31.11	13.72	12.21	18.5
Cr	12.17	0.52	50.94	0.62
Al	3.85	0.74	1.18	0.71
Sn	1.96	0.37	0.01	0.46
Hf	0.93	2.17	2.00	2.49
Si	1.11	37.38	10.18	36.66

In the extruded condition, recrystallization of the β phase occurred and there was some alignment of silicide phase with the extrusion direction Fig. 3(d), the vertical direction is parallel to the extrusion direction). Again as in alloy #1, the extrusion process apparently did not break up the silicide phase.

For alloy #2, another extrusion was carried out at 1400°C/6:1 ratio in an attempt to impart a high plastic deformation to the silicide phase at a higher extrusion temperature. Fig. 4 (a) and (b) show the microstructures in the as extruded and as-extruded + 1350°C/24 h HTed conditions. The horizontal direction in these micrographs is the extrusion direction. Like the extrusion at 1350°C, the 1400°C extrusion appears not to deform (or breakup) the silicide phase to any significant extent.

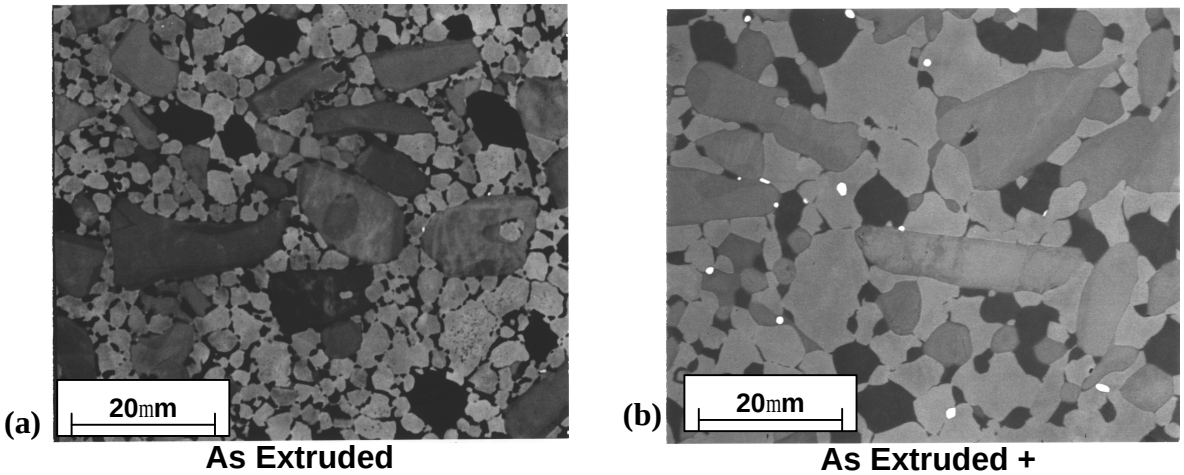

Figure 4. Microstructure of (a) hot extruded (1400°C/6:1 Ratio) and (b) hot-extruded and heat treated alloy #2 (Table II).

The microstructures in the as cast, as cast + HTed, and extruded conditions for the alloy #3 are shown in Fig. 5 (a), (b) and (c). Because of high Si content (16.8 at %), there is a high volume fraction of hypereutectic silicide phase in the as cast condition. In this alloy also the hot-extrusion did not deform the silicide phase appreciably. The EPMA data for phase chemistry are given in Table VI; the major phases present are the metallic β phase, the Nb-rich 5:3 silicide and the Ti-rich 5:3 silicide.

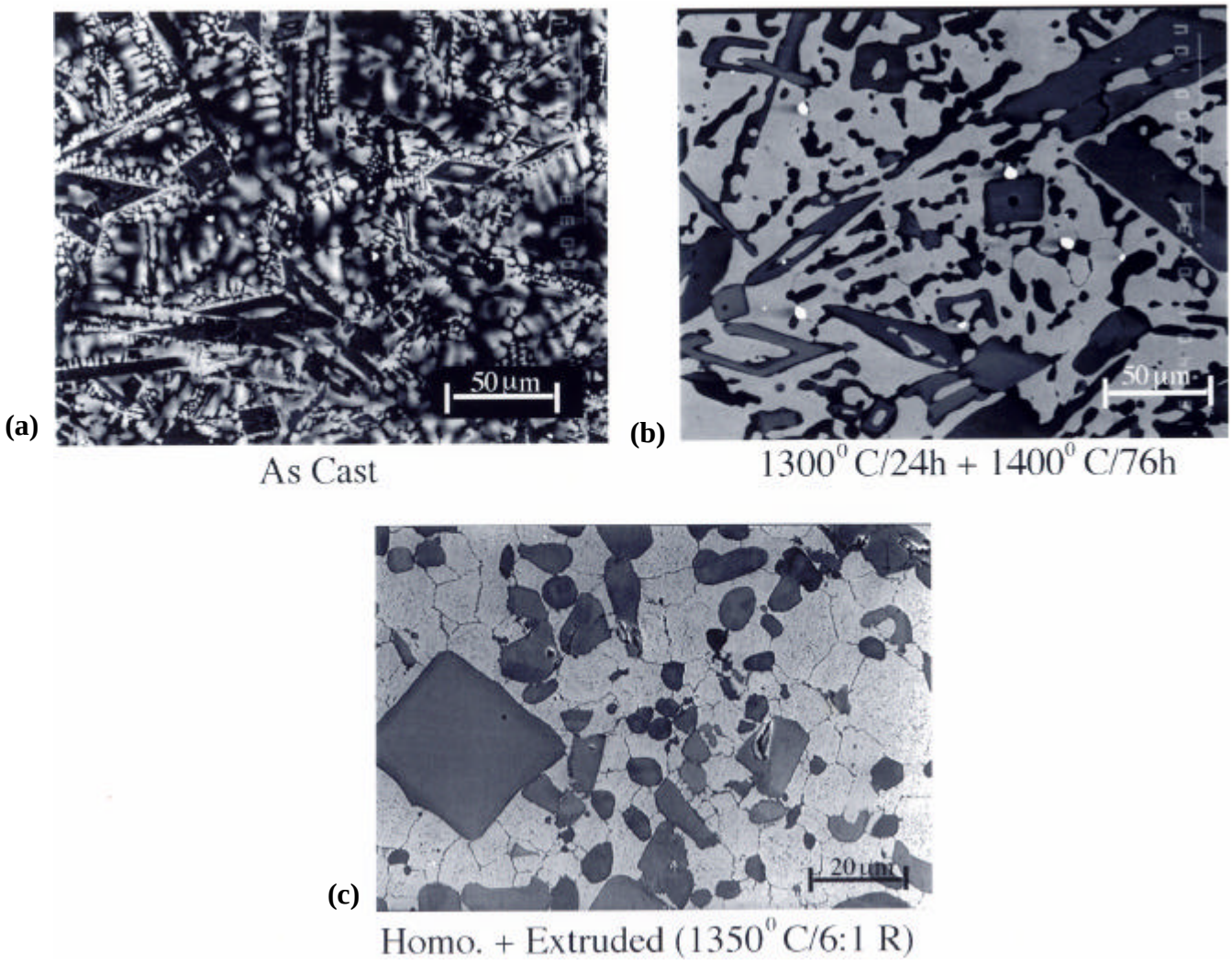

Figure 5. Microstructural development in alloy #3 (Table II) in the (a) as cast, (b) homogenized and (c) hot-extruded (1350°C/6:1 ratio) conditions)

Table VI
Phase Chemistry as Revealed by EPMA for Alloy #3 (At%)

7.3Cr - 16.8Si (1300°C/24 h + 1400°C/76h)

Element	b Phase	$(NbTi)_5Si_3$	$(TiNb)_5Si_3$
Nb	52.85	45.15	27.14
Ti	29.08	14.14	27.14
Cr	12.55	0.32	1.37
Al	1.69	0.36	0.81
Sn	1.62	0.32	0.1
Hf	1.07	1.99	5.52
Si	1.14	37.73	37.41

For alloy #4, which was a second ISM trial to obtain target levels of Si and Ge in the castings, hot-extrusion was done after a homogenization treatment of 1300°C/24 h + 1350° C/76 h. The microstructures of as-cast, and homogenized alloy are shown in Fig. 6(a) & 6(b). The cast microstructure has a high volume fraction of a silicide phase. The homogenization treatment coarsened the microstructure somewhat. The phases present, as determined by EPMA (Table VII) were: metallic β phase, Nb and Ti rich 5:3 silicides and Cr2Nb phase. The extrusion, Fig. 6(c), again did not break up or plastically deform the silicide phases to any significant extent. The extruded alloy was further heat treated at 1400°C/8 h + 1550°C/2 h; no melting was detected

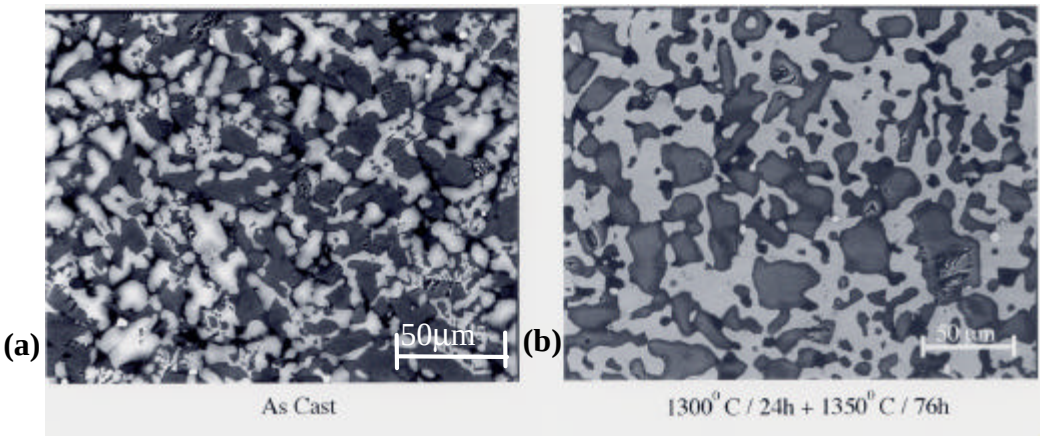

Figure 6. The microstructure in alloy #4 (Table III) in the (a) as-cast and (b) homogenized conditions

Table VII – Phase Chemistry as Revealed by EPMA for Alloy #4 (At%)

6.2Cr - 11.Si - 4.06Ge (1300°C/24h + 1350°C/76h)

Element	b Phase	$(NbTi)_5Si_3$	$(TiNb)_5Si_3$	Cr_2Nb
Nb	59	44.2	23.03	37
Ti	24.62	15.63	13.14	21.8
Cr	7.46	1.54	36.52	1.89
Fe	1.75	2.50	14.1	2.56
Al	1.27	1.85	3.39	2.64
Sn	0.55	22.7	7.02	21.35
Hf	0.23	9.2	0.83	10.11
Si	3.12	1.68	1.96	1.82
Ge	1.98	0.61	0.01	0.74

Based upon this result it was decided to heat treat a billet at progressively increasing temperatures up to 1500°C and then extrude it at 1475°C/10:1 ratio to find out whether extrusion at higher temperature/ratio will produce a refined silicide microstructure. This was done, however, the results showed no refinement of microstructure.

For the extruded + heat treated alloys, the volume fractions and average sizes of the major phases were determined from the SEM micrographs using standard lineal analysis. These data are given in Table VIII.

Table VIII
Volume Fractions and Average Sizes of the Main Phases

Alloy # and Chemistry		b Phase		(NbTi)5Si3		(TiNb)5Si3		Cr2Nb	
		f	Size	f	Size	f	Size	f	Size
#1	7.3Cr - 3.7Fe-12.8Si-1.06Ge	44%	55 mm	44%	60 mm Blocky	-	-	8%	25 x 8 mm Platelets
#2	14.3Cr - 14.4Si	38%	40x25 mm	38%	75 x 25 mm Long Blocky	-	-	15.5%	30 x 10 mm
#3	7.3Cr - 16.8Si	50%	Cont. ?	40%	120 x 40 mm	9%	10 mm	-	-
#4	6.2Cr - 2.8Fe - 11Si - 4.6 Ge	44.5%	~13 mm Irregular	48%	15 mm Irregular	-	-	7%	7 mm

7. Powder Consolidation and Characterization:

As far as we know, for the present complex, multi-component Nb alloys, no rapidly solidified powders have been produced. Therefore, this is a first attempt to make powders in sufficient quantity for evaluation of engineering properties. As mentioned earlier, six electrodes

with a total weight of ~38 lb were manufactured by the ISM process. Powders were produced by PREP method which yielded -35 mesh powders of ~ 9lb. Large angular chunks fell-off during powder making, which were probably not rapidly solidified. This may be due to presence of brittle silicide phases and presumably porosity and crack-like defects present in the electrodes. To make powders, the electrodes were spun between 9000-10,000 RPM; this high speed may result in enough centerfugal force to break parts of electrodes. We are in discussion with Starmet personnel to improve the powder processing and increase the powder yield for future powder making by this method. Alternatively, we are exploring the possibility of gas-atomization of the melt (Crucible, Inc.) to produce powders. Because of limitation of crucible size for melting, at present Nb-based powders can be produced using the gas-atomization process in small batches up to ~ 5lb.

Fig. 7(a-d) shows the microstructures in the -35 mesh PREP powders. The powder particles exhibited a variety of microstructures.

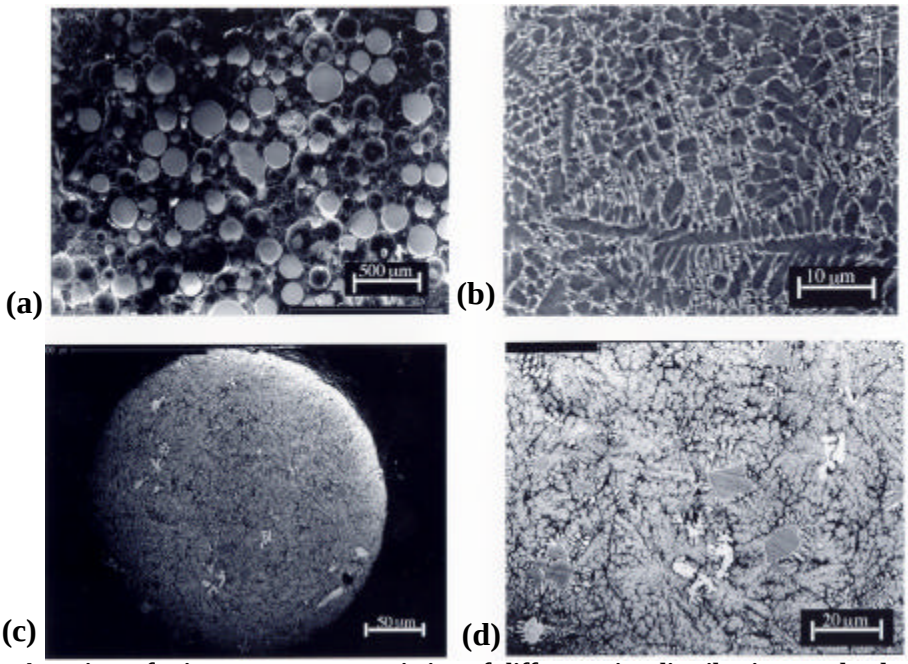

Figure 7. A variety of microstructures consisting of different size distributions and volume fractions of the Nb_{ss} and silicide phases were seen in different PREP powder particles. (Alloy #4, Table III).

Fig. 7(b) shows a microstructure, which has high volume fraction of Nb-rich 5:3 silicide while Fig. 7(c) & (d) show particles containing a mixture of hypereutectic silicide phase (gray angular constituent) and a very fine eutectic of Nb phase and silicides. In addition, angular chunks (<500 μm in size) of almost ~ 100% silicide phase were found. Thus, this powder did not provide all particles possessing very fine rapidly solidified multiphase microstructure with uniform chemistry. It is possible that process improvement, or alternatively, gas-atomization

The PREP powders were extruded in Mo cans at 1350°C and 1400°C, both at 10:1 ratio. External appearance of both extrusions looked good and metallographic examination revealed full consolidation. Fig. 8(a) & (b) shows the microstructure of the 1400°C extruded material. The low magnification micrograph 8(a), shows that the Si-rich powder particles did not deform during extrusion. The surrounding material, Fig. 8(b) shows a microstructure consisting of a fine mixture of 4 main phases: β Nb solid solution, Nb- and Ti-rich silicides and Cr_2Nb Laves phase. Microstructure also contained very fine HfO_2 (bright) particles. Thus some microstructural refinement is possible using P/M route provided Si-rich powder particles can be avoided during powder making by Hot Extrusion.

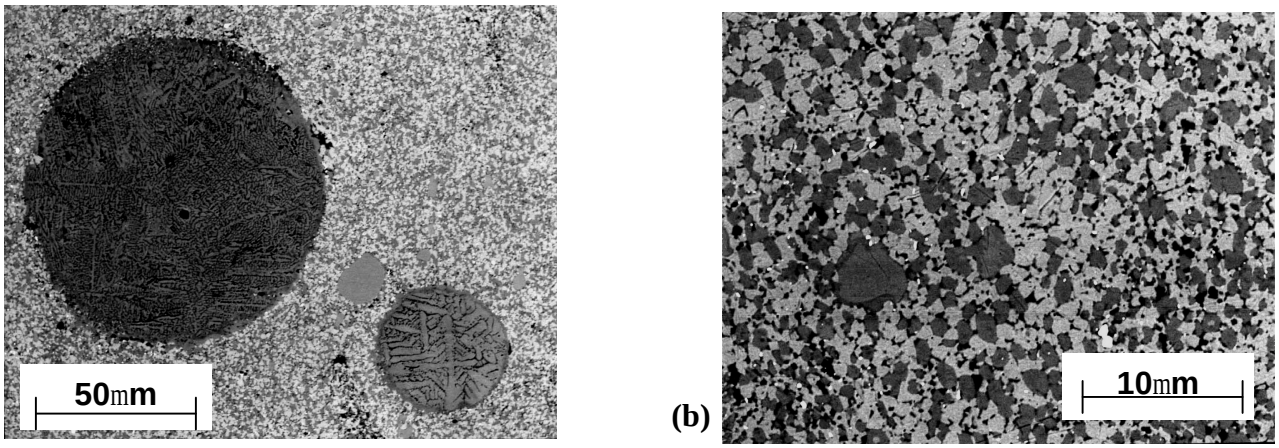

Figure 8. Extruded (1400°C/10:1) PREP powder microstructure (a) large Si-rich particles did not deform during extrusion and (b) the surrounding uniform and fine mixtures of Nb_{ss} and intermetallic phases.

Only a small quantity (~300 gm) of gas-atomized powders could be obtained from Crucible. The main reason for the small yield is the formation of a thick skull in the crucible even though a charge of 5 lb of prealloyed chunks was melted. Due to high melting temperature of the Nb-based alloy, Crucible has only a small experimental facility to atomize the powders. Fig. 9 shows –35 mesh powder particle shapes and size distribution.

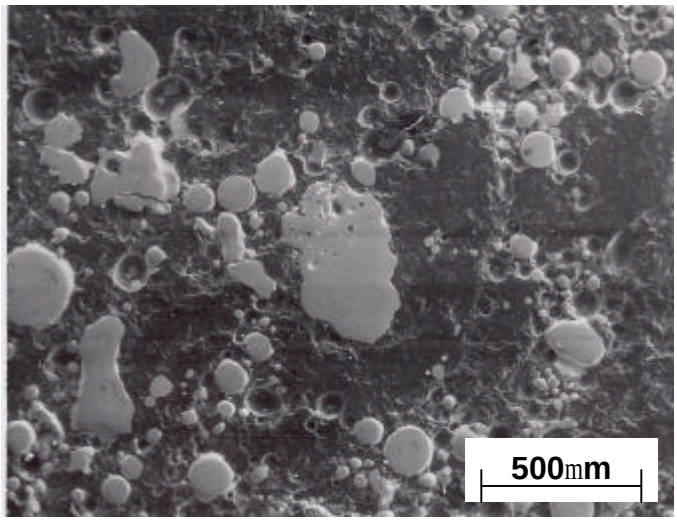

Figure 9. The –35 mesh gas-atomized particles (alloy #4, Table III) exhibited a variety of shapes and sizes.

It can be seen that while the smaller particles are spherical, there are a significant number of irregular shaped larger particles containing different volume fractions, sizes and shapes of Silicide and βNb phases.

Fig 10(a) and (b) exhibit an irregular shape particle containing a high volume fraction of the primary 5:3 silicide phase (gray) and a dark region (roughly in the center of the photographs) which is very rich in Si.

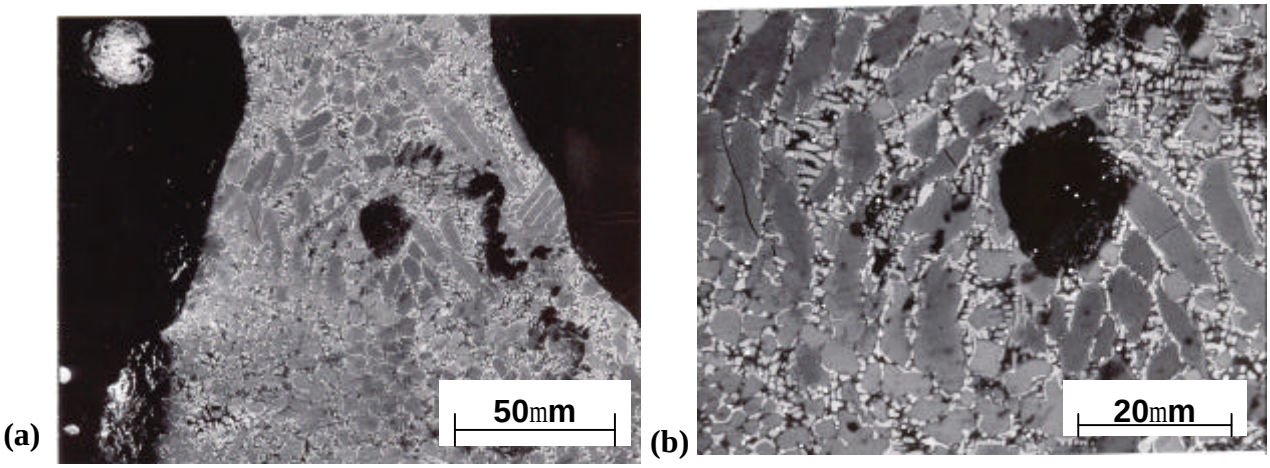

Figure 10. Microstructure within an irregularly shaped gas-atomized particle consisting of a high fraction of silicide phase (gray), Nb_{ss} (bright) and a Si-rich (dark) region.

Fig.11(a) and (b) show microstructure within a spherical particle consisting of a fine mixture of 5:3 silicide (gray) and Nb_{ss} (bright) phases. Thus, the powder particles did not show uniform chemistry or microstructures.

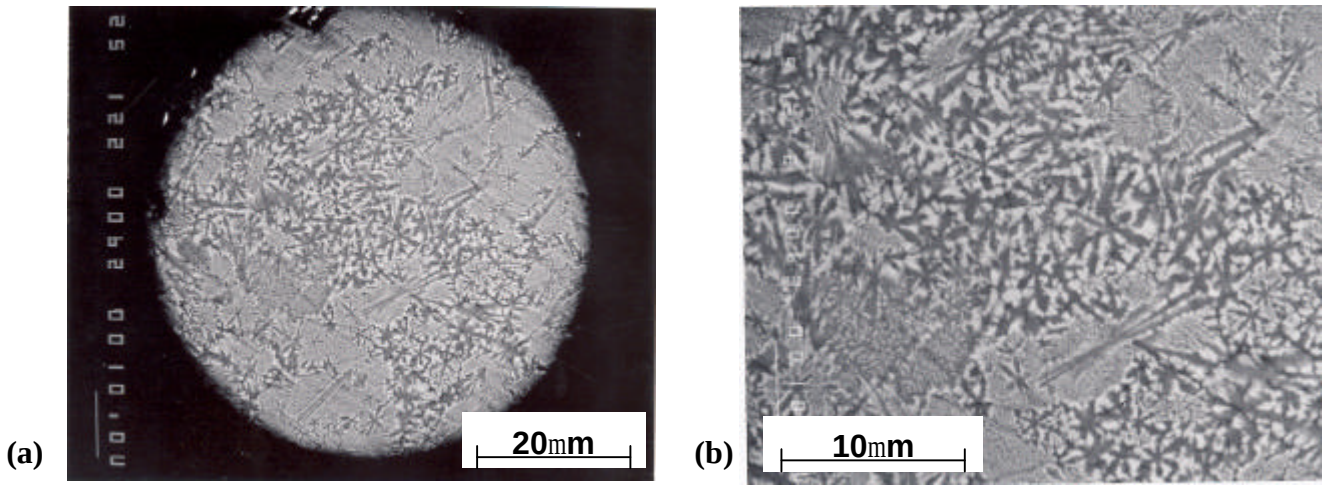

Figure 11. A fine spherical gas-atomized particle containing fine mixture of silicide (gray) and Nb_{ss} (bright) phases.

Since only a small amount of gas-atomized powder was at hand, it was decided to consolidate the powder by hipping (rather than by hot-extrusion). The powder was canned in a 2mm thick Nb tube and degassed in vacuum at 500°C for 2 h before sealing the can. The

hipping cycle consisted of 1350°C for 6 h in argon pressure of 210 MPa. Metallographic examination revealed nearly fully consolidated powder with a very low fraction of isolated pores ~ 2μm diam. The decanned samples were further heat treated at 1350 and 1400°C for 24h and at 1500°C/8 h in an inert atmosphere to homogenize the microstructure as much as possible.

Fig. 12(a) and (b) are the electron back–scattered SEM micrographs showing typical examples of microstructures in the as-hipped and 1400°C/24 h heat treated condition. The microstructure consisted of large (~50 μm) silicide particles (indicated by arrow, Fig 12(a)) and a uniform fine mixture of Nb_{ss} and intermetallic 5:3 silicides and Laves phases. The phases present were essentially same as those present in alloy #4 (Table VII). However, as compared to as-cast + hot-extruded microstructures (Fig. 6) the gas-atomized powders exhibited some degree of microstructural refinement.

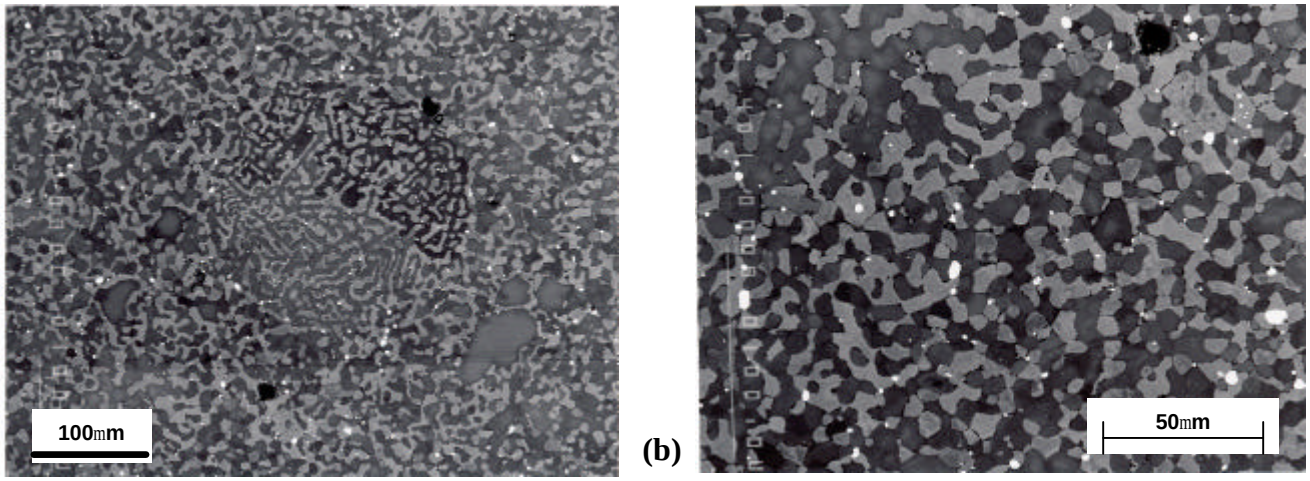

Figure 12. Microstructure in the hip consolidated (1350°C/6h/210MPa argon pressure) + heat-Treated (1400°C/24h) gas-atomized powder. Large (~50mm) silicide particles and a uniform mixture of Nb_{ss} and silicide phases were present.

8. Mechanical Properties:

Compression, tension and toughness tests were carried out from room temperature to 1100°C in air for the extruded alloys. The data are presented in Table IX, the alloy compositions are denoted by Cr, Si, Fe and Ge levels. The compressive yield strengths were high at RT and 800°C (1550-1600 MPa and ~ 1500 MPa, respectively), dropped to between 500-600 MPa at 1000°C and dropped further to 200-270 MPa at 1l00°C. The compressive ductilities were ~ 3% at room temperature, and, from 800 - 1100°C, the alloys were very ductile. In contrast, tensile tests showed no ductility at room-temperature and 800°C, slight ductility at 1000°C (~ 0.5%) and considerable ductility at 1100°C (> 5%). Thus these materials exhibit a brittle-to-ductile transition temperature >1000°C. The tensile fracture strengths were much lower from RT to 1000°C in comparison to the corresponding compressive yield strengths; this indicates that the tensile strengths are limited by the premature brittle failure. Extensive fractography on failed tensile samples indicated that the fracture was mainly controlled by brittle failure of largest or agglomerated silicides. Considerable refinement of silicide phases by innovative processing (including powder metallurgy) is required to increase the tensile strengths.

Table IX
Mechanical Properties of Extruded Alloys

Compressive Yield Strength (MPa)					
Alloy #	**Alloy Composition**	**RT**	**800°C**	**1000°C**	**1100°C**
1	**7.3Cr – 3.7Fe – 12.8Si – 1.06Ge**	**1587**	**1503**	**550**	**260**
2	**14.3Cr – 14.4Si**	**1629**	**1492**	**540**	**240**
3	**7.3Cr – 16.8Si**	**1654**	**1528**	**600**	**270**
4	**6.2Cr – 2.8Fe – 11Si – 4.6Ge**	**1567**	**1487**	**500**	**210**

Fracture Strength (s_f) and Yield Strength ($s_{0.2}$) (MPa)					
Alloy #	**Alloy Composition**	**RT***	**800°C***	**1000°C****	**1100°C****
1	**7.3Cr – 3.7Fe – 12.8Si – 1.06Ge**	**225, 134**	**190, 225**	**185**	**170**
2	**14.3Cr – 14.4Si**	**390, 203**	**280, 340**	**372, 357**	**187**
3	**7.3Cr – 16.8Si**	**250, 345**	**332**	**360, 365**	**219**
4	**6.2Cr – 2.8Fe – 11Si – 4.6Ge**	**227, 303**	**294**	**260**	**138**

* Fracture Strength (~ zero ductility)
** Yield Strength
{ Duplicate tests in some cases

Toughness (K_Q) (MPaÖm)					
Alloy #	**Alloy Composition**	**RT**	**800°C**	**1000°C**	**1100°C**
1	**7.3Cr – 3.7Fe – 12.8Si – 1.06Ge**	**8.6, 6.0**	**7.8**	**8.4**	**7.7**
2	**14.3Cr – 14.4Si**	**10.1, 10.1**	**10.9**	**11.8**	**14.6**
3	**7.3Cr – 16.8Si**	**10.6**	**11.87**	**12.96**	**16.69**
4	**6.2Cr – 2.8Fe – 11Si – 4.6Ge**	**9.5, 9.3**	**8.9**	**8.8**	**6.64**

The high Si containing alloys (#2 & #3) had a room-temperature fracture toughness of ~ 10 MPa√m, increasing somewhat from 1000°C and reaching values between 14.6 to 16.7 MPa√m at 1100°C. The Ge containing alloys (#4) had lower toughness values at room temperature and they decreased slightly with increasing temperature.

9. Fractographic Observations

Extensive SEM examination was carried out in secondary electron mode on fracture surfaces of tensile samples tested from room-temperature to 1100°C. The microconstituents (i.e. Nb_{ss}, silicides etc) were identified on the fracture surfaces by energy dispersive x-ray analysis (EDAX) to determine their failure modes.

For the extruded alloys (Table II), the room temperature fracture occurred in brittle low-energy mode for the Nb_{ss} as well as for the intermetallic phases. Fig. 13(a) is an example of low magnification appearance of fracture for alloy #2, a high proportion of large flat facets are apparent as well as a low fraction of regions exhibiting some tearing. The Nb_{ss} phase fractured mostly in a cleavage mode, Fig.13(b) shows a characteristic cleavage-like river pattern (bright grain in the center of the picture). The intermetallic phases exhibited mixed transgranular/intergranular brittle fracture. Fig. 13(c) depicts the transgranular fracture through the 5:3 silicide phase, exhibiting a low energy, very flat appearance. Secondary cracking is also seen in the silicide phase. Very rarely, some local regions of Nb_{ss} phase failed in mixed ductile dimple/quasi cleavage mode.

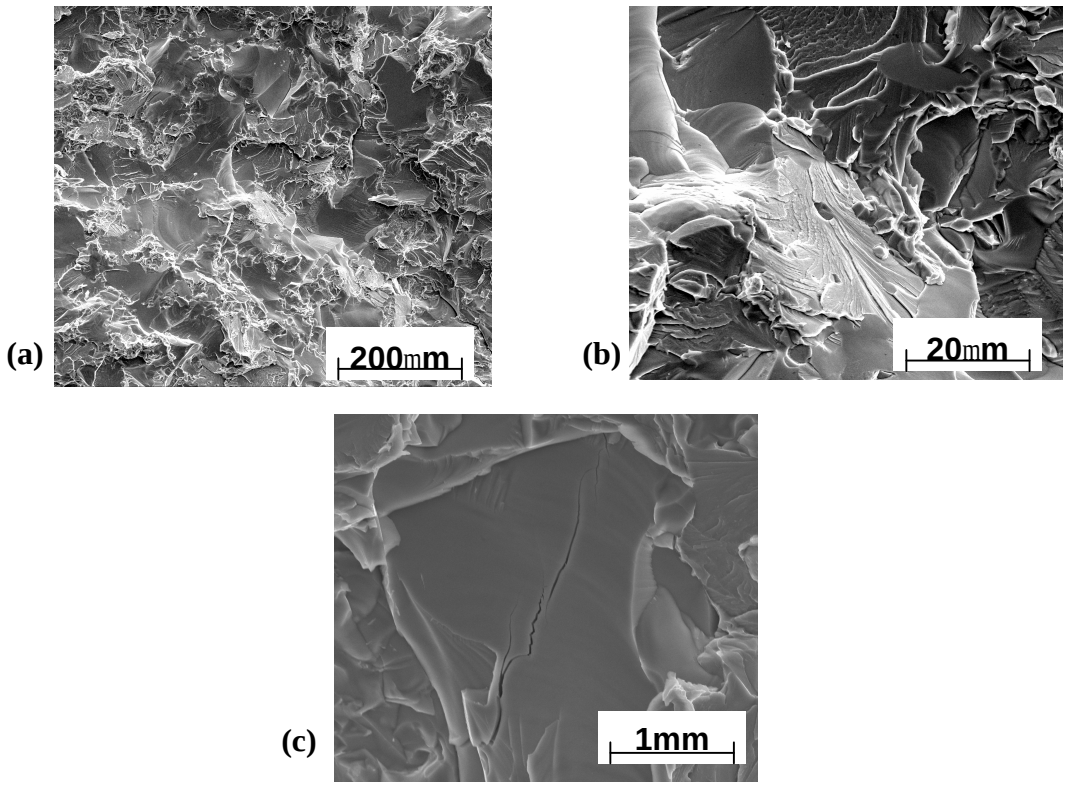

Figure 13. SEM Fractographs exhibiting an example of brittle failure for all the alloys tested at room temperature, (a) low magnification picture consisting of a high proportion of flat facets and indications of limited tearing (b) cleavage-like fracture of Nb_{ss} (bright centered grain) and (c) very flat, low energy fracture mode through the silicide phase.

Fig. 14(a), (b) and (c) show a Nb_{ss} grain at progressively higher magnifications, exhibiting portion of fracture consisting of fine dimples and portion showing cleavage like features. The high magnification micrograph, Fig. 14(c), exhibits particles at dimple centers. These particles, which may be responsible for nucleating these dimples, have not been identified; they are most probably Cr_2Nb (Laves) phase particles precipitating in the supersaturated Nb_{ss} solid solution during cooling.

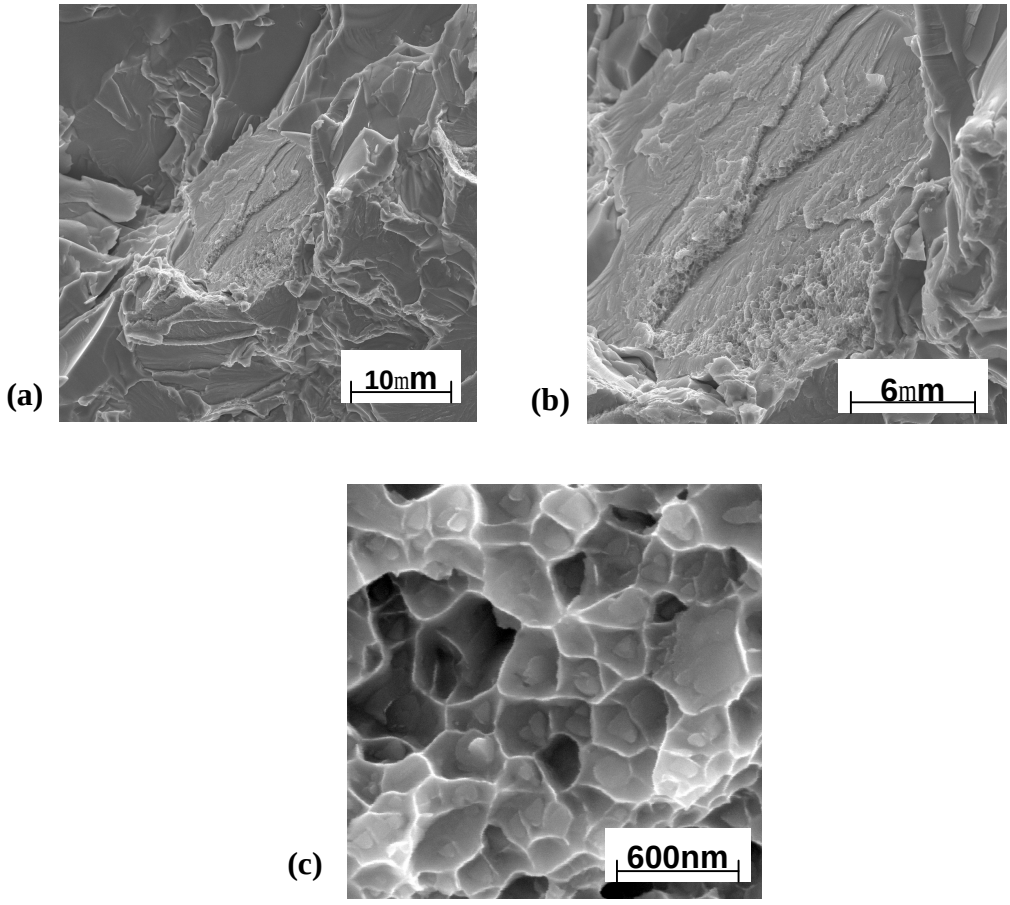

Figure 14. (a) – (c) show a rare example of mixed cleavage and ductile dimple regions in a Nb_{ss} grain for room-temperature fracture of alloy #1

The observation of room-temperature brittle fracture modes in various phases for the extruded alloys is consistent with the premature tensile failures with low fracture strengths and no ductility. Fractography of tensile specimens tested at 800°C showed appearance of brittle failures as shown in the low magnification micrograph, Fig. 15(a). At high magnification, Fig. 15(b), there are some indication of microplasticity of the Nb_{ss} phase (arrows) but it was not sufficient to provide macroscopic ductility.

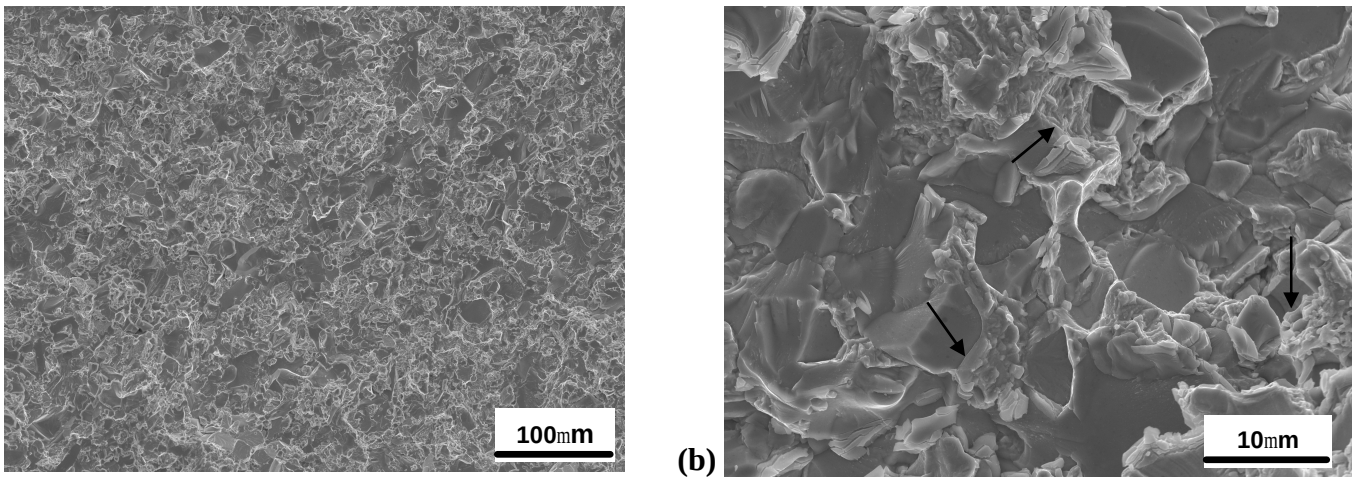

Figure 15. (a) Fracture features at 800°C also indicated brittle failure, (b) indication of limited microplasticity in the Nb_{ss} phase (bright features) at 800°C.

At 1100°C, the extruded alloys showed significant tensile plasticity; fracture surface observations revealed that a significant portion of Nb_{ss} phase failed in a ductile dimple mode. Fig. 16(a), at low magnification, shows the fracture features; arrows A indicate ductile failure of the Nb_{ss} phase. At some locations (arrow B), the Nb_{ss} phase fractured in cleavage mode, while the intermetallic phases (arrow C), even at 1100°C, exhibited low-energy brittle failure facets. Fig. 16(c) shows, in greater detail, the ductile dimples in the Nb_{ss} phase with nucleating particles in their centers.

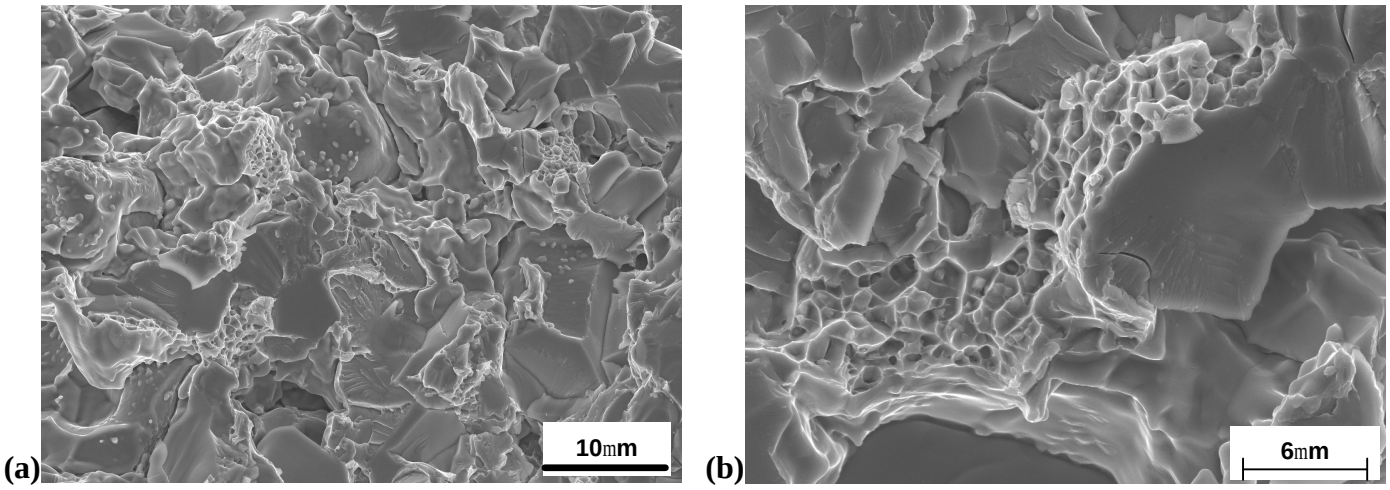

Figure 16. 1100°C fracture features for alloys exhibiting considerable tensile ductility. A high fraction of Nb_{ss}

Longitudinal metallographic sections of the failed tensile samples were examined by SEM to further define damage mechanisms near the main fracture. The general features of cracking were similar for all the extruded alloys, thus variations in chemistry of alloys did not have an effect on the fracture processes. Figs. 17(a)-(d) give examples of cracking in the tensile samples tested at room temperature. Fig. 17(a) shows profuse cracking of silicides just below the main crack with Nb_{ss} phase relatively intact. Fig. 17(b) and (c) give examples of cracks in the silicides which stop at the Nb_{ss} phase. There were many such observations signifying crack trapping by the Nb_{ss} phase. No evidence of interphase debonding was seen. Of course, for tensile samples to fracture, the trapped cracks must eventually tranverse the Nb_{ss} (or link up by other mechanisms e.g. crack briding). Fig. 17(d) provides an example of relative straight traces of cracks (cleavage) through the Nb_{ss} phase. Observations did not reveal crack-bridging to be significant.

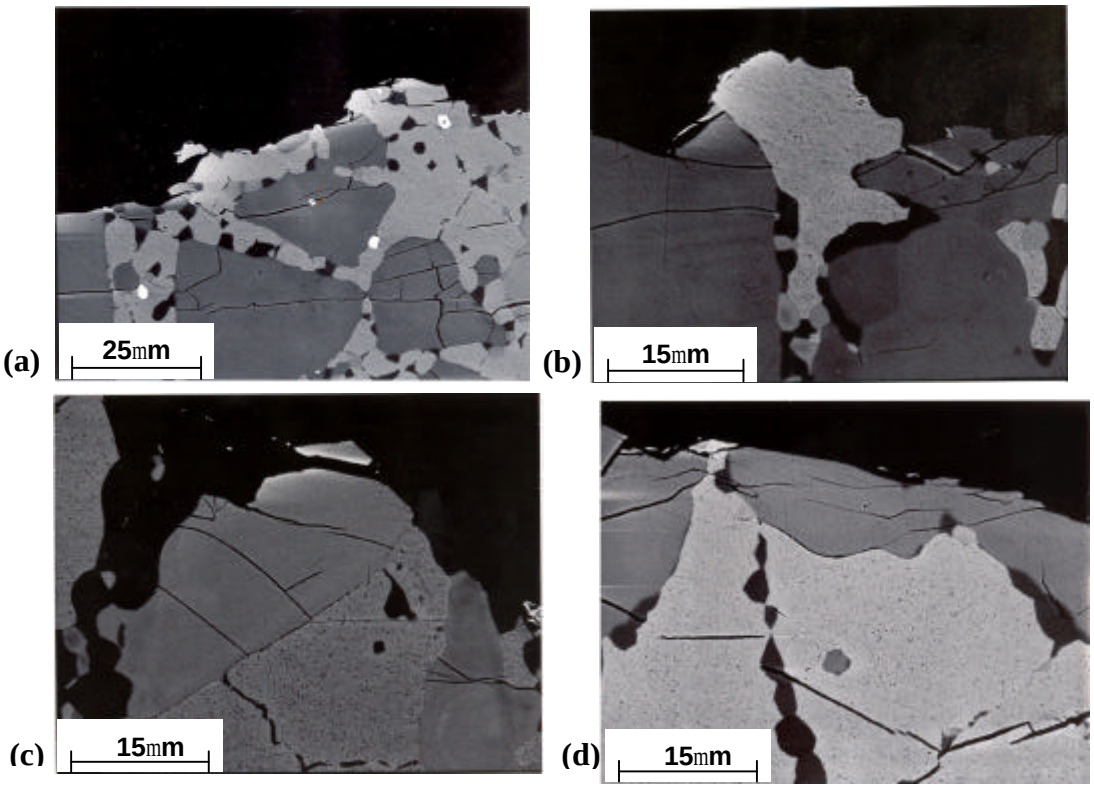

Fig 17. Examples of various fracture mechanisms at room temperature as revealed by SEM examination of longitudinal failed sections. (a) profuse silicide cracking with intact Nb_{ss} phase, (b) and (c) illustrations of silicide cracks stopping at the Nb_{ss} phase (crack trapping), (d) straight cleavage cracks through the Nb_{ss} phase.

For the high temperature tests (1000 and 1100°C), observations of the longitudinal sections revealed significant internal oxidation of the surface Nb_{ss} phase even for short durations of the tensile tests (heating rate = 8°C/min, 20 minutes of equilibration time at temperature and testing time of ~ 1 min at 1000°C, 5 min at 1100°C). Generally, the internal oxidation can cause considerable hardening and embrittlement of the Nb_{ss} due to dissolved oxygen (to saturation solubility limit) and due to precipitation of mixed oxides of Ti and Nb, and SiO_2. Fig 18 shows a longitudinal section of a tensile sample tested at 1000°C. The tensile loading was in the horizontal direction. A zone of ~ 20 μm of internally oxidized Nb_{ss} (mottled contrast shown by arrows) can be seen. As exemplified in this picture, the cracking was mostly confined to the silicide phase, this behavior was seen at numerous locations for a number of samples tested at 1000 and 1100°C. These observations indicated that the silicide phase was much more weaker and brittle in tension than the internally oxidized Nb_{ss}.

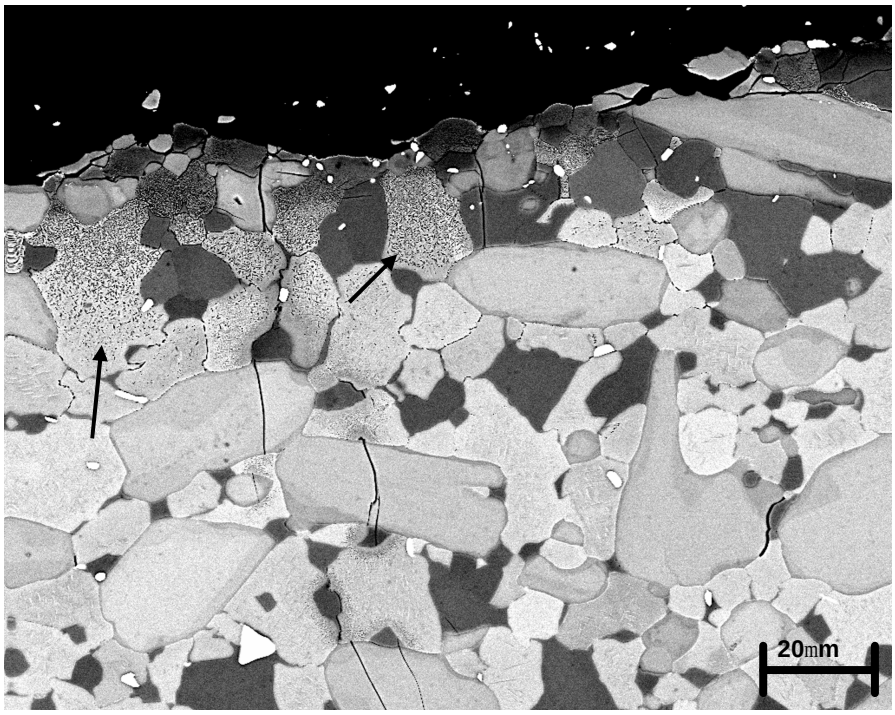

Fig 18. Longitudinal section of a failed sample at 1000°C showing internal oxidation of the Nb_{ss} phase (mottled contrast, arrows). Cracks were generally found in the silicide phase rather than in the internally oxidized Nb_{ss} phase.

There was only one observation where the oxidized Nb_{ss} might have fractured in preference to the silicide phase, this is shown in Fig. 19.

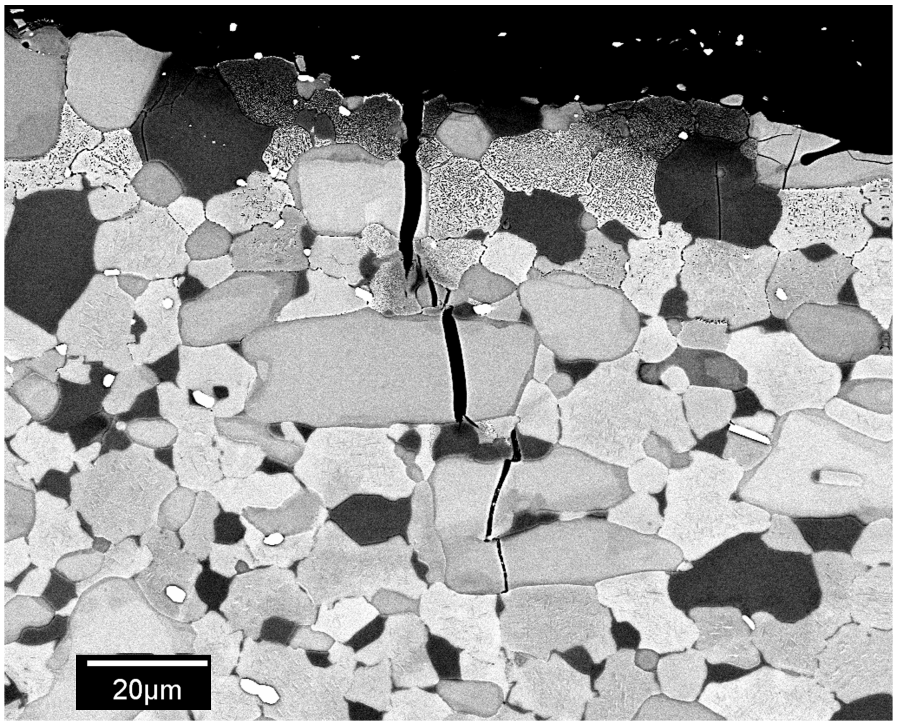

Fig 19. A rare observation of fracture occurring through the internally oxidized Nb_{ss} phase at 1000°C.

A few room-temperature tensile tests were carried out on PREP hot-extruded material. The microstructure of this P/M consolidated alloy is given in Fig. 8 and described earlier in this report. The room-temperature fracture strengths ranged from 118-169 MPa (3 specimens); the low strengths are attributed to presence of large brittle Si-rich powder particles, undeformed during hot-extrusion. Figs. 20(a), (b) and (c) show SEM fractographs of one of these specimens (σ_f = 159 MPa). The low magnification picture Fig. 20(a) shows large Si-rich spherical particles (~ 100 – 250 µm diam. in this picture) which show dark contrast surrounded by lighter fracture features. Fig. 20(b) shows, at higher magnification, very brittle fracture through the dark particle; EDAX revealed this particle to be 5:3 silicide. Fig. 20(c) and (d) show the surrounding

multi-phase fracture features exhibiting a significant degree of plastic tearing of the Nb_{ss} phase (bright features).

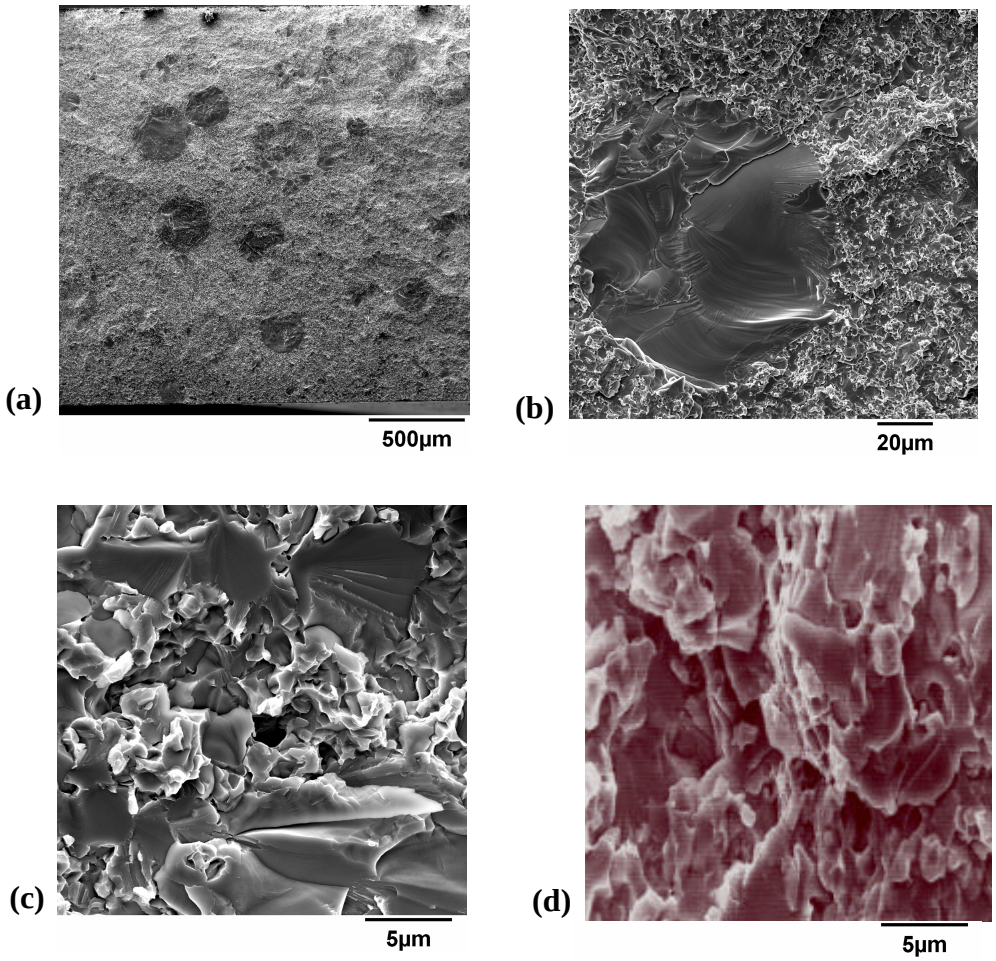

Fig 20. Room-temperature fracture features for a failed hot-extruded PREP powder specimen (a) low-magnification picture showing dark Si-rich spherical particles surrounded by the lighter fracture features (b) the Si-rich particles failed in a highly brittle fashion (c) and (d) surrounding multiphase fracture with tearing and dimples in the Nb_{ss} phase.

These observations indicate that there is possibility of considerable energy dissipation by plasticity of the Nb_{ss} phase in the fine microstructure. If during powder processing the large Si-rich phase particles can be avoided , then it is possible to enhance the fracture strength significantly.

10. Calculations for Toughening and Strength

Toughness: A number of toughening mechanisms can be considered in case of the present brittle/ductile multiphase alloys. They include "extrinsic" mechanisms such as crack bridging, microcracking, crack branching or deflection. Cracks which nucleate and traverse the brittle phases can be trapped by the ductile phase and further propagation can occur by crack renucleation across or bowing around the ductile phase. This provide intrinsic toughening for the system. It should also be mentioned that a volume of the ductile phase immediately in the vicinity of the hard phase experiences high plastic constraint from triaxial hydrostatic stresses induced by the non-deformable hard phase. This constraint can significantly reduce dissipation of energy at the crack tip trapped by the constrained ductile phase, thus reducing the amount of possible toughening.

The observations of damage/fracture processes in the present alloys (described earlier) do not indicate dominance of a single toughening mechanism. In addition, based upon the microstructural appearance (Figs. 2-5) and the volume fractions of the phases (Table VIII) it is difficult to delineate which is the matrix phase and which is the dispersed phase. Crack trapping (Fig. 17) seems to be a possible toughening mechanisms. In absence of a clear dominant mechanism, a simple rule-of-mixtures for toughness of these alloys can also be considered. Therefore, based upon available models from literature, calculations are made for the room-temperature toughness based upon crack-trapping and rule-of-mixtures. Even though, there is no clear evidence of crack-bridging, for the sake of completeness, calculation is also included for this mechanism. The calculated values are then compared with experimentally determined values.

1. Crack Trapping Toughening

(a) Unconstrained Ductile phase.

Bower and Ortiz [4] have modeled the toughening due to crack-trapping and bowing by ductile particles in a brittle matrix. The toughness of the composite, K_c, is given by:

$$K_c = K_I \left\{ 1 + \frac{2r}{l} \left[\left(\frac{K_d}{K_I} \right)^2 - 1 \right] \right\}^{1/2}$$

where K_I = toughness of the hard intermetallic phase

K_d = toughness of the ductile phase

$2r$ = average size of the trapping phase

l = average spacing between the ductile phase

From microstructures (Fig. 2-5) $\frac{2r}{l}$ can be taken to be ~1, $K_d = 18\text{MPa}\sqrt{\text{m}}$ and $K_I = 2.5\text{MPa}\sqrt{\text{m}}$. These toughness values for Nb_{ss} and the intermetallic silicide phases are taken from literature for compositions very close to those in the present alloys [5,6]. The calculation yield the composite toughness of $18\text{MPa}\sqrt{\text{m}}$. The experimental value is ~ $10\text{MPa}\sqrt{\text{m}}$ (Table IX, alloys #2 and #3). Thus, this model overestimates the experimental value. The model assumes crack trapping and bowing in an idealized microstructure (array of spherical ductile particles in a brittle matrix) to be the dominant mechanism, which is not necessarily the case for the present alloys. Additionally, the model does not take into account the plastic constraints in the ductile phase imposed by the hard intermetallic phase.

(b) Constrained Ductile Phase:

Recently Chan and Davidson [7] have derived the following expression for toughness where strong intermetallic phase constrains the plasticity of the ductile phase:

$$K_c = K_I \left[1 - \sqrt{1-f} \left(\left[\frac{K_d}{K_I} \right]^2 \exp\left\{ -\frac{8q}{3} \left(\frac{f}{1-f} \right) \right\} - 1 \right) \right]^{1/2}$$

In this equation f is the volume fraction of the ductile phase (≈ 0.45 for Nb_{ss}, Table VIII) and q is a material constant ≈ 1 [5]. Here the composite toughness K_c can be calculated for two cases i) the entire volume of the Nb_{ss} is fully constrained (i.e., f = 0.45) and ii) the constraint is experienced by ductile phase only in the vicinity of the silicide/Nb_{ss} interface, in this case it is assumed that only half the volume of the Nb_{ss} is constrained and other half is fully ductile with negligible hydrostatic stress state. This means that the effective volume fraction of the ductile phase is ~0.225. Taking these values for fully constrained and partially constrained Nb_{ss}, the calculated K_c values are 5.3 and 11.5 $MPa\sqrt{m}$, respectively. The latter value is very close to the experimental K_c of ~ 10 $MPa\sqrt{m}$.

2. Rule-of-Mixture (ROM) Toughness

Again according to Chan and Davidson [7], the ROM toughness is given by:

$$K_c = K_I \left[f + (1-f) \left(\frac{K_d}{K_I} \right)^2 \right]^{1/2}$$

for f =0.45 for Nb_{ss}, this K_c value calculates to be = 13.45 $MPa\sqrt{m}$.

3. Crack-Bridging Toughening

As stated earlier, there is no evidence of crack bridging as a major toughening mechanism in the present alloys. However, it is instructive to determine the magnitude of such toughening for the overall microstructure, and size and volume fraction of the ductile Nb_{ss} phase. Under the assumption of small-scale bridging, the estimate of toughness is given by [8]:

$K_c = \left[K_I^{\,2} + fE'\sigma_o r\chi\right]^{1/2}$ where:

$E' = E/(1-v^2)$, the plane-strain elastic modulus with E = elastic modulus

v = poisson's ratio.

σ_o = Yield Strength of Nb_{ss}

χ = constraint factor

r = half the average size of the $Nb_{ss} \approx 50\mu m$

Values of σ_o and E' are not known for the present multicomponent solid –solution Nb_{ss}, however these values are known for the binary Nb_{ss} for the Nb-Si system [6]. For Nb saturated with Si, σ_o = 386 MPa and $E' \approx 150$ GPa. The parameter χ signifies the strength of constraint experienced by the Nb_{ss} because it is bonded to the silicide phase. For many systems this parameter is shown to range from 1-6, the smaller numbers signify strong bond [9]. Since at room-temperature no interphase debonding was observed in the failed tensile sample for the present alloy, the value of χ is taken to be unity. The calculated value of K_c is 36.4 $MPa\sqrt{m}$, this is much higher than the experimentally determined value of ~ 10 $MPa\sqrt{m}$. The high value of crack-bridging toughness is due to a large volume fraction (~0.45) and large size (~ 100 μm) of the fairly strong Nb_{ss} phase.

11. Fracture Strength

The measured room-temperature tensile fracture strength values vary widely from 134 to 390 MPa among different compositions (Table IX). The fracture is elastic and, most likely, the brittle silicide phase agglomerates cause failure initiation. A simplistic calculation of the fracture strength can be made using standard linear fracture mechanics approach where: $s_f = \dfrac{K_c}{1.12\sqrt{\pi C}}$

here 2C is the size of the penny shape internal flaw. If it is assumed that the fractured silicide

phase acts as the strength-controlling flaw, then the largest size of silicide agglomerate can be measured from the microstructure. This value is of the order of ~ 200 μm, although statistical distribution curve (specially tail end for largest particles) has not been determined. Taking $2C \approx 200$ μm and $K_c \approx 10$ MPa$\sqrt{m}$, the calculated σ_f value is 504 MPa, which is higher than maximum experimentally determined value of ~ 390 MPa. It should be noted that there are many factors which affect this calculation: i) residual stresses due to thermal expansion mismatch or anisotropy are not taken into account ii) experimental value of K_c is determined on notch bend bars without notch-tip sharp crack; the plane-strain K_{IC} value may be lower than K_c value used iii) some of the largest flaw sizes have not been determined statistically and iv) the internal state of stress for the multi phase material may be very complex with triaxialities and sharp gradients. Thus, a simplistic approach involving continuum linear fracture mechanics which ignore intricacies of the microstructure may not be appropriate in predicting fracture strength.

12. Summary and Conclusions:

a. Induction skull melting (ISM) processing is a viable method for making cast ingots with reasonable physical integrity and chemistry control. At present, the major limitation of this method is the small size of melting crucible in which only 11.36 Kg of charge can be melted. Scale-up will require significantly larger crucible and associated higher power for melting the refractory Nb-base alloys.

b. The high levels of Si and Si + Ge (≥ 14 at%) in the selected alloys produce large primary silicide phases in the cast ingots. These phases are brittle and contain porosity/crack-like defects, which are not eliminated by long-term hipping at 1400°C/210 MPa pressure. More aggressive

hipping cycles may eliminate these defects, however, they have not been explored in the present work.

c. Hot extrusions done at 1350, 1400 and 1475°C at extrusion ratio's of 6:1 and 10:1 did not result in break-up and extensive plastic deformation (i.e. shape change) of the silicide phases.

d. P/M route together with hot-extrusion has been attempted to refine the microstructures. Both the PREP and gas-atomized powders contained non-uniform microstructures; many powder particles contained high volume fractions of large silicides (~20 μm) which were not broken up by subsequent hot extrusions.

e. A uniform and fine as-cast multi-phase microstructure is possible if the Si content is very close to a eutectic composition. For the present family of alloys, this Si level is ~ 12 at %.

f. The present alloys possess high compressive yield strength values (~1500 MPa at room temperature and 800°C, 500-600 MPa at 1000°C, and 210-270 MPa at 1100°C). However tensile testing revealed that the alloys were totally brittle up to 800°C (zero plasticity) with large variation in fracture strength from 134-390 MPa. Fracture toughness values were weakly dependent on composition and temperature and were in the neighborhood of $\sim 10 \mathrm{MPa}\sqrt{\mathrm{m}}$. Fractographic analysis revealed that the large silicide agglomerates crack readily and are responsible for the brittle failures of these alloys. The Nb_{ss} phase provides some degree of damage tolerance by trapping the cracks, although below 1000°C, this phase exhibits mainly the cleavage fracture mode.

13. References

1. P.R. Subramanian, M.G. Mendiratta, and D.M. Dimiduk; Journal of Metals, 1996, Vol. A239-240, pp 1-13.

2. P.R. Subramanian, M.G. Mendiratta, D.M. Dimiduk and M.A. Stucke; Mater. Sci. Eng., 1997, Vol. A239-240, pp. 1-13.
3. B.P. Bewlay, M.r. Jackson, J.-C. Zhao, P.R. Subramanian, M.G. Mendiratta and J.J. Lewandowski: accepted for publication in MRS Bulletin “in press” (September 2003, devoted to “Ultrahigh Temperature Materials for Jet Engines).
4. A.F. Bower and M. Ortiz; J. Mech Phys. Solids 1991; 39: pp 815-58.
5. R.M. Nekkanti and D.M. Dimiduk; Mat. Res. Soc. Symp. Proc., Pittsburgh, PA, Vol. 194, 1990, pp 175-182.
6. M.G. Mendiratta, J.J. Lewandowski, and D.M. Dimiduk: Metall. Trans. A., Vol 22A, 1991, pp. 1573-1583.
7. K.S. Chan and D.L. Davidson: Metall. Mater. Trans. A. 2001, Vol 32A, pp 2717-27.
8. H.E. Deve, A.G. Evans, G.R. Odette, R. Mehrabian, M.L. Emiliani, and R.J. Hecht: Acta Metall. Mater., 1990, Vol. 38, pp 1491-1502.
9. P.A. Mataga: Acta Metall., 1989, pp 3349-59.